



HAL
open science

Real-Time Analysis of Magnetic Hyperthermia Experiments on Living Cells under a Confocal Microscope

Vincent Connord, Pascal Clerc, Nicolas Hallali, Darine El Hajj Diab, Daniel
Fourmy, Véronique Gigoux, Julian Carrey

► **To cite this version:**

Vincent Connord, Pascal Clerc, Nicolas Hallali, Darine El Hajj Diab, Daniel Fourmy, et al.. Real-Time Analysis of Magnetic Hyperthermia Experiments on Living Cells under a Confocal Microscope. *Small*, 2015, 11 (20), pp.2437-2445. hal-01990950

HAL Id: hal-01990950

<https://insa-toulouse.hal.science/hal-01990950v1>

Submitted on 8 Jul 2024

HAL is a multi-disciplinary open access archive for the deposit and dissemination of scientific research documents, whether they are published or not. The documents may come from teaching and research institutions in France or abroad, or from public or private research centers.

L'archive ouverte pluridisciplinaire **HAL**, est destinée au dépôt et à la diffusion de documents scientifiques de niveau recherche, publiés ou non, émanant des établissements d'enseignement et de recherche français ou étrangers, des laboratoires publics ou privés.

DOI: 10.1002/ ((please add manuscript number))

Article type: Full Paper

Real-time Analysis of Magnetic Hyperthermia Experiments on Living Cells under Confocal Microscope

Vincent Connord[#], Pascal Clerc[#], Nicolas Hallali, Darine El Hajj Diab, Daniel Fourmy, Véronique Gigoux, and Julian Carrey**

V. Connord, N. Hallali, Dr J. Carrey

Université de Toulouse ; INSA ; UPS, Laboratoire de Physique et Chimie des Nano-Objets (LPCNO), F-31077, Toulouse, France, and CNRS ; UMR 5215 ; F-31077 Toulouse, France

P. Clerc, D. El Hajj Diab, Dr D. Fourmy, Dr V. Gigoux

Université de Toulouse 3, EA 4552, Toulouse, France

* Corresponding authors: Julian Carrey, LPCNO, 135 avenue de Rangueil, F-31077 Toulouse, France. Email: julian.carrey@insa-toulouse.fr and Véronique Gigoux, EA 4552, CHU Toulouse, Avenue du Professeur Jean Poulhès, F-31432 Toulouse, France. Email : Veronique.Gigoux@inserm.fr

[#] These authors contributed equally to this work.

Keywords: magnetic nanoparticles, magnetic hyperthermia, confocal microscope, cell death, reactive oxygen species.

Combining high-frequency alternating magnetic fields (AMF) and magnetic nanoparticles (MNPs) is an efficient way to induce biological responses through several approaches: magnetic hyperthermia, drug release, controls of gene expression and neurons, or activation of chemical reactions. So far, these experiments could not be analyzed in real-time during the AMF application. A miniaturized electromagnet fitting under a confocal microscope is built, which produces an AMF of frequency and amplitude similar to the ones used in magnetic hyperthermia. AMF application induces massive damages to tumoral cells having incorporated nanoparticles into their lysosomes without affecting the others. Using this setup, real-time analyzes of molecular events occurring during AMF application are performed. Lysosome membrane permeabilization and reactive oxygen species production are detected after 30 min only of AMF application, demonstrating they occurs at an early stage in the cascade of events leading eventually to cell death. Additionally, lysosomes self-assembling

into needle-shaped organization under the influence of AMF is observed in real-time. This experimental approach will permit to get a deeper insight into the physical, molecular and biological process occurring in several innovative techniques used in nanomedicine based on the combined use of magnetic nanoparticles and high-frequency magnetic fields.

1. Introduction

Magnetic hyperthermia has been the subject of an active research activity in the past decade and tremendous progresses have been made in basic research on this promising cancer treatment.^[1] Very large heating powers have been reached using magnetic nanoparticles (MNPs) which are either chemically-synthesized^[2,3] or extracted from bacteria,^[4] driven by a better understanding of the way to optimize heat generation.^[5] Receptor-ligand grafted nanoparticles which are able to bind specifically to receptors overexpressed at tumoral cell surface and then internalize through receptor-dependent pathway have been developed.^[6,7,8] The combination of MNPs and alternating magnetic field (AMF) application has been shown to induce cell death in many *in vitro* experiments^[6,7,8,9,10] and to induce tumor regression of xenografted tumors in mice.^[4,11,12,13] It has been shown that efficient targeting of tumors in mice could be accomplished after intravenous injection, which constitutes a real milestone.^[12,13] Finally, accumulation and degradation mechanisms of MNPs once in cells or biological tissues have been studied in details.^[14,15] In spite of these successes, the basic mechanisms leading to cell death in AMF treatments is still unclear. Indeed, several experiments have reported that cells die in spite that there is no perceptible temperature rise during experiment.^[6,7,8,9,10,16] This finding brings a lot of hope for the future of this treatment since it makes possible to induce cell death with a very low amount of MNPs^[8,17] and, interestingly, makes possible to envisage eradicating small metastatic tumors or circulating tumoral cells in addition to large primary tumors. Elucidating the cellular and molecular mechanisms at the origin of cell death in these experiments is one major quest in this therapeutic approach.

The standard instrument in cell biology to analyze cellular and molecular mechanisms during *in vitro* experiments is the fluorescence confocal microscope. Combined with the numerous available fluorescence probes, pharmacological agents of signaling pathways, it permits to gain a deep insight into the cell machinery. In particular, during AMF treatments, the capacity of fluorescence confocal microscopes to image cell behavior in real-time could be used to detect *in situ* several physical, chemical and biological events which are associated at the origin of cell death: temperature increase, [18] pH variations, lysosomal membrane permeabilization, reactive oxygen species (ROS) generation, membrane fluidity modifications, [19] molecule motion and activation of cell death signaling pathways could thus be spatially and temporally detected.

Unfortunately, so far, confocal microscope has not been used at its full capacity in magnetic hyperthermia studies. It has been mainly used before AMF treatment to measure MNPs internalization, perform post-endocytotic trafficking studies and as a post-treatment characterization tool. In fact, the time period of AMF application in itself has always stayed so far inaccessible to confocal microscope imaging. The two main reasons for this are that i) most AMF inductors used in laboratories are bulky coils which cannot fit under a microscope due to the small space available, and ii) even if a way was found to do so, the presence of the high-frequency magnetic field could heat the ferromagnetic parts of the microscope in the vicinity of the sample.

In the present article, we describe a successful approach to achieve real-time cell imaging during AMF treatments of tumoral cells. It is based on the application of a localized high-frequency magnetic field using a miniaturized electromagnet. The potentialities of the new setup are illustrated by i) data showing that the rate of cell damage, leading eventually to cell death, achieved *in situ* using this device are similar to the previous ones obtained on the same tumoral cells using standard coils, ii) evidence that cell damage is an event occurring at the single-cell level and is dependent on the presence of internalized MNPs in lysosomes, iii) data

showing a dynamical study of the lysosome membrane permeabilization and ROS formation during AMF treatment, iv) dynamical experiments of lysosome alignments which form inside certain cells when the AMF is applied. This AMF inductor will certainly enable to quickly get key informations on the mechanisms at the origin of the death of cells containing minute amounts of receptor-driven internalized MNPs. More generally, it should give a new start to all topics in biology and nanomedicine where high-frequency AMF are used.

2. Results

2.1. Fabrication and characterization of the miniaturized electromagnet.

The electromagnet is a miniaturized version of the setup described in Ref. [20]. It has been elaborated by machining a small commercial ferrite core. 3D schematics and picture of the electromagnet are shown in Figure 1(a) and S1. It is composed of a 400 μm gap with a V-shape enlargement permitting to avoid the shadowing of the gap during experiments under microscope. To define a flat working area, a plane was polished at approximately 45° of the tore plane. A system of screws was added inside the ferrite core to adjust the planarity of the working area. The driving coil is composed of 12 turns of Litz wire. An adjustable capacitor is placed in series with the electromagnet to reduce its high frequency impedance which equals 0.66Ω at 300 kHz.

A standard way of evaluating the AMF produced by the electromagnet could have been to measure it using a Hall probe when a dc current is injected into the coil. Then, measuring the ac current during AMF application would have been sufficient to know the AMF amplitude. This method has proven to be very reliable for large gap electromagnets^[20] but cannot be applied here due to the small width of the gap compared to the Hall probe thickness. To evaluate the magnetic field amplitude $\mu_0 H_{\text{max}}$, three complementary approaches were used. Evaluation was done when a peak current $I_{\text{max}} = 1.5 \text{ A}$ was sent into the coil, since these are

the conditions of the AMF treatment (see below). The first method uses the following equation, valid when the relative permittivity inside the gap equals 1:

$$\mu_0 H_{\max} = \frac{\mu_0 N I_{\max}}{\frac{S_{\text{gap}} L_{\text{core}}}{S_{\text{core}} \mu_{\text{core}}} + L_{\text{gap}}} \quad (1)$$

where N is the number of turns of the coil, μ_{core} the relative permittivity of the ferrite, L_{core} (L_{gap}) the length/width of the ferrite (gap) and S_{core} (S_{gap}) the section of the ferrite (gap). Due to the large permittivity of the ferrite, the first term at the denominator of the equation is small and leads to only a small correction compared to the standard equation $\mu_0 H_{\max} = \frac{\mu_0 N I_{\max}}{L_{\text{gap}}}$.

For $I_{\max} = 1.5$ A, the calculated magnetic field is $\mu_0 H_{\max} = 60 \pm 4$ mT. The second one consists in using a home-made miniaturized pick-up coil of diameter 3.5 mm to measure directly the ac magnetic field amplitude (see Figure S2). Its diameter is such that it completely fits into the gap. An AMF $\mu_0 H_{\max} = 46 \pm 3$ mT is thus measured at $f = 300$ kHz and $I_{\max} = 1.5$ A. The third method consisted in using finite elements simulations to calculate the magnetic field using the exact gap geometry. A map of the magnetic field is shown in Figure 1(b). A profile of the magnetic field into the gap is also shown in Figure 1(c). The magnetic field amplitude is homogeneous on all the gap section with a value of 58.0 ± 0.5 mT. Measured and calculated values of AMF amplitude are of the same order of magnitude, and the AMF amplitude is likely to be in the range 46-60 mT. In the remaining, we will use the mean value in this range $\mu_0 H_{\max} = 53$ mT.

2.2 AMF application to living cells under a confocal microscope.

The nanoplatform used in magnetic hyperthermia experiments (termed DY647-MNP-gastrin) is composed of commercial iron oxide nanoparticles coated with PEG-Amine and decorated

with i) a synthetic replicate of gastrin, which binds specifically to the cholecystokinin-2 receptor (CCK2R), a receptor overexpressed in endocrine tumors, and allows specific MNPs internalization in cells overexpressing the CCK2R, ii) a fluorescent label (DY647).^[5] All experiments were performed on living cells in a CELLview (see below). To apply the AMF under the confocal microscope, the electromagnet is placed so its polished part is in contact with the CELLview. The whole is put under the fluorescence confocal microscope, which is equipped with a heating plate. An environmental chamber is then built around the CELLview to maintain a homogeneous temperature during the experiments. A picture of the complete setup is shown in Figure S1(c). In these conditions, generating an ac current of 1.5 A in the driving coil, corresponding to an AMF of 53 mT in the electromagnet gap, requires a power of 1.5 W and rises the chamber temperature to approximately 34°C. A 37°C temperature is maintained during the experiments by manually adjusting the heating power of the plate. Figure 1(d) shows an infrared picture of the electromagnet and of the medium taken during dedicated experiments performed outside the microscope. These experiments are more detailed in the Materials and Methods section and in Figure S3. There is no significant temperature gradient in the medium. Moreover, the temperature difference between the medium and the ferrite near the gap is approximately 1°C. Infrared observations of the setup at the end of typical experiments under the microscope confirm the results obtained in air. It can be safely concluded that the temperature is quite homogeneous in the CELLview during AMF treatments.

2.3. Selective damage to cells having internalized targeted magnetic nanoparticles.

For these experiments, cells having or not internalized DY647-MNP-gastrin were harvested, mixed and suspended in agar gel. The gel containing the mixture of cells was poured into the CELLview once the electromagnet was in place. A magnetic field of 53 mT was applied during 2 hours. The CELLview was then put back into an incubator during 4 hours, and the

impact of magnetic field treatment was then determined by counting cells labeled with prodidium iodide, corresponding to cells with a damaged membrane.^[5] Typical pictures of cells inside and outside the gap are shown in Figure 2(a). As shown in Figure 2(b), applying the AMF during 2 hours selectively caused damages to cells having internalized MNPs. Indeed, inside the gap, 72.1 ± 9.5 % of cells having internalized targeted MNPs were damaged comparatively to 18.4 ± 6.3 % of cells devoid of MNP ($p < 0.001$). Of note, outside the gap, 20.0 ± 1.7 % and 12.5 ± 4.1 % of cells containing or not targeted MNPs were damaged ($p = 0.23$). Two important conclusions can be drawn from these experiments. First, the fact that the same damage rate was observed for tumoral cells devoid of MNPs inside the gap ($p = 0.21$) or containing MNPs outside the gap ($p = 0.11$) comparatively to control cells (without MNPs and outside the gap) confirms that the miniaturized electromagnet does not cause significant cell damage due to eventual temperature rise or to other unpredictable reasons. Second, the fact that, in an intimate mix of cells containing targeted MNPs or not, only the ones containing DY647-MNP-gastrin were damaged when submitted to an AMF is a clear proof that cell damages are in no case related to a global temperature rise, but to mechanism(s) occurring at the single cell level, dependant on both presence of MNPs inside the cells and delivery of the AMF to these cells. This supports the conclusion that this mechanism(s), whatever it is, can be used to destroy individual cells without being harmful to their neighbors, at the condition that the targeted cell contains MNPs. Finally, percentage of cells positive to prodidium iodide obtained with the miniaturized electromagnet is slightly higher than the previous ones obtained on the same tumoral cells using a 52 mT AMF treatment applied with a standard coil.^[6] This might indicate that the AMF amplitude is in the upper part of the range [46-60] mT of estimated values rather than its middle.

2.4. Real time capture of lysosomal membrane permeabilization.

Following first biological experiments which confirmed that our electromagnet enables to kill tumoral cells having internalized gastrin-grafted MNPs, we pursued the study by analyzing magnetic field-induced lysosomal membrane permeabilization, which is an event likely to play an important role in cell death.^[6, 7] For this purpose, a gel containing cells having internalized DY647-MNP-gastrin and accumulated the lysosomal fluorescent probe LysoTracker was used. The effect of magnetic field was evaluated by recording the lysosome staining intensity by confocal microscopy and by image analysis of colocalization between LysoTracker and DY647-MNP-gastrin, provided by Pearson's coefficient. During each experiment, series of pictures were taken every 30 minutes in predefined zones inside and outside the gap corresponding to cells treated or not by the AMF, respectively. Figure 3 shows typical pictures of the experiments as well as the evolution of Pearson's coefficient over the time. In absence of AMF, Pearson's coefficient reflecting DY647-MNP-gastrin and LysoTracker colocalization was 0.59 ± 0.03 and 0.55 ± 0.04 in cells outside and inside the gap respectively [see Figure 3(a)]. During AMF application, DY647-MNP-gastrin and LysoTracker colocalization decreases significantly in cells inside the gap unlike cells outside the gap. After only 30 min of AMF treatment, the difference is statistically significant (0.55 ± 0.03 outside and 0.45 ± 0.03 inside the gap, $p = 0.039$). This reveals that lysosome membrane permeabilization is an early phenomenon in the events induced by the AMF treatment and leading eventually to cell death. After 90 mn of AMF treatment, Pearson's coefficient values are 0.46 ± 0.05 outside the gap and 0.26 ± 0.07 inside ($p = 0.021$), indicating that AMF treatment induced specifically leaking of lysosome content of cells having internalized MNPs.

2.5. Imaging of ROS production.

Lysosomal membrane permeabilization induced by an alternating magnetic field is correlated with the production of reactive oxygen species (ROS).^[7] We performed assays to record AMF-induced production of ROS in cells having incorporated DY647-MNP-gastrin using

CellRox green reagent by fluorescence confocal microscopy. ROS production was analyzed on adherent cells inside and outside the gap as the AMF was applied during 120 min. Typical micrographs of cells inside and outside the gap are shown in Figure 4(a). The time evolution of ROS production is shown in Figure 4(b). Fluorescence intensity increased significantly in cells submitted to the AMF compared to the cells outside the gap. The fluorescence intensity ratio after 30 min of AMF treatment is significantly different (2.9 ± 1.4 higher comparatively to control cells), indicating that ROS production is early phenomenon in the events induced by the AMF treatment. It occurs concurrently with lysosomal membrane permeabilization and leads eventually to cell death. After 100 min of AMF treatment, ROS production ratio reaches a maximum value with 3.9 ± 1.3 -fold higher production comparatively to control cells. Although it has been shown previously that ROS production increased during AMF treatment,^[7] it is the first time that its dynamic of production could be measured.

2.6. Lysosome alignments under AMF.

During experiments described in the previous sections, we observed in some cells fluorescent needles which are aligned in the direction of the applied magnetic field. They correspond to lysosomes which self-assembled due to magnetic dipolar interactions. Figure 5 illustrates dynamical experiments in which the AMF was successively switched on and off while observing such a cell. These needles scatter into small individual fluorescent dots when the AMF is off and self-assemble again when the AMF is on (Figure 5). Assembling and disassembling occurs within a few minutes, although assembling seems faster. The fact that these needles are not observed in all cells is not understood so far. Possible explanation might be that, in cells where needles are observed, lysosomes could move more easily due to a loss of cytoskeleton organization and/or that these cells are the ones where lysosomes contain more targeted MNPs. These unexpected results illustrate the interest of real-time imaging to get access to events which could not be observed otherwise. These observations will also

make possible to evaluate the degree of magnetic interactions between lysosomes and to take them into account when calculating the heating power of MNPs once inside cells.

3. Discussion

Elucidating the cascade of events leading in the end to cell death in magnetic hyperthermia is a major task in this field, especially since it is known that, in many experiments, global temperature increase is not at the origin of cell death.^[6, 7, 8, 9, 10, 16] Important results have been obtained toward this goal: i) Evidence of ROS generation during application of AMF has been previously reported using flow cytometry performed at the end of the AMF application.^[7, 21] ii) Membrane permeabilization was previously evidenced by the decrease of lysosomal acridine orange intensity and the release of lysosomal cathepsin B into the cytosol.^[7] We show here that using a miniaturized electromagnet, such events can be monitored dynamically under a confocal microscope during AMF treatment. It is shown that these two processes occur at the very first stage of the AMF treatment, well before cell death could be detected. The fact that membrane permeabilization revealed by LysoTracker occurs early is thus a supplementary indication that the cell death triggering signal may be initiated in the lysosome compartment, where the targeted MNPs were accumulated. On one other hand, the role of the ROS production during AMF treatment is more complex to state and two hypotheses can be formulated: i) membrane permeabilization of lysosomes could be initially caused by the formation of ROS into the lysosomes through the well-known Fenton reaction.²² In our experiments, possible ROS generation into lysosomes could not be detected using the present method which was based on cell accumulation of ROS-sensitive fluorescent probe. ii) ROS production might be a consequence of lysosome permeabilization. This hypothesis is compatible with the multiple sources of ROS formation in cells, including mitochondria, peroxisome, or endoplasmic reticulum. As an alternative cause of lysosome membrane permeabilization, mechanical forces exerted by MNPs must be considered, in particular in the

light of a recent report showing that lysosomal membrane-bound MNPs cause lysosome disruption under a slowly rotating magnetic field ^[23] or that MNPs might vibrate at high-frequency during AMF application. ^[24] Future experiments will address this important question of sub-cellular localization of ROS production during AMF treatment of tumoral cells containing MNPs, which could permit to clarify the pathways leading to cell death. The miniaturized electromagnet presented here will be a precious tool for elucidating these basic mechanisms.

An important additional issue in AMF treatment concerns temperature measurements. Several progresses on real-time or indirect measurements of temperature at the surface of magnetically heated nanoparticles have been done in the past few years. ^[25, 26, 27, 28] The present setup is compatible with the use of molecular thermometers based on fluorescence emission intensity and could make possible intracellular temperature measurements during AMF application, which has not been realized so far.

Finally, the combination of MNPs and high-frequency AMF has been used to trigger the release of drugs from liposomes or polymer nanobeads, ^[29, 30, 31, 32] control gene expression ^[33], activate enzyme reactions ^[34] or activate neurons. ^[25] Here again, real-time monitoring could lead to several advances in these promising fields related to magnetic hyperthermia.

4. Conclusion

We have successfully developed a way to submit cancer cells to a high frequency AMF under a confocal microscope. The magnetic field frequency and amplitude are in the range of the ones used in classical magnetic hyperthermia experiments and other related topics where high-frequency AMF are used to induce biological responses. Using this setup, an AMF was applied on a gel containing tumoral cells having or not internalized MNPs, which did not induce a global temperature increase. The fact that cell damage was seen exclusively in the cells containing targeted MNPs validates the setup; it also shows that cell damage occurs at a

single-cell level and is dependent on both AMF and presence of the MNPs in the cells. Real-time capture of two events suspected to play a key role in cell death induced by the magnetic field treatment were performed: lysosomal membrane permeabilization and ROS generation. These two phenomena are detected after 30 mn of AMF treatment only and thus occur at an early stage in the cascade of events leading eventually to cell death. We have also observed that, in some cells, lysosomes having accumulated MNPs could self-organize into needles under the influence of the AMF. This novel experimental approach is simple to develop and widely opens the field of experiments which could be undertaken to get an insight into the cellular and molecular mechanisms occurring during AMF application on living cells.

4. Experimental section

Electromagnet fabrication. A commercial ferrite core with an internal (external) diameter of 19 (29) mm and a thickness of 7.5 mm was used as starting point for the electromagnet elaboration (TN29/19/7.5-3C90, Ferroxcube). A thin slit was first created using a diamond saw, leading to a gap of approximately 400 μm . Starting from the mid-height of this slit, a V-shape enlargement of the gap was machined using a rotating grinding wheel. Then, a plane at approximately 45° with respect to the core plane was polished at the gap level to define a flat working area. A system of plastic screws was added inside the ferrite core so the planarity of the electromagnet can be adjusted. The electromagnet was wound with 12 turns of Litz wire ($24 \times 10 \times 0.05$, Connect systemes). An adjustable capacitor was built by replacing the capacitors of a standard decade box (DC05, ELC) by high-voltage ceramic disk capacitors (Panasonic, MDU series; Murata, DE series; Epcos, B81123 series). The electromagnet and the capacitor box were put in series. The high-frequency current was produced by a voltage amplifier (HSA 4052, NP Corporation) driven by a function generator (MTX 3240, Metrix). The current in the setup was measured with an AC current probe (3274 clamp probe, Hioki) connected to an oscilloscope (TDS 2022B, Tektronix). The applied

voltage was measured at the output of the amplifier using the same oscilloscope. At a working frequency of 300 kHz, the capacitor values required to bring the electromagnet to resonance equals 12 nF.

Magnetic field evaluation. To calculate the AMF value and its incertitude using Equation (1), the following parameters were used: $\mu_{\text{core}} = 3000 \pm 300$ was extracted from the ferrite constructor datasheet, $L_{\text{core}} = 75.1 \pm 0.5$ mm, $L_{\text{gap}} = 370 \pm 3$ μm , $S_{\text{core}} = 41 \pm 3$ mm², $S_{\text{gap}} = 13.7 \pm 1.0$ mm² and $I = 1.5 \pm 0.1$ A. The pick-up coil was elaborated by winding 2 turns of a 200 μm in diameter wire on a 2.7 mm in diameter cylinder rod in order to form a flat spiral. A picture of the coil is shown in Figure S2. The peak voltage appearing at the coil terminals \mathcal{E} was measured using an oscilloscope (TDS 2022B, Tektronix). Peak magnetic field $\mu_0 H_{\text{max}}$ was evaluated using the formula $\mu_0 H_{\text{max}} = \frac{\mathcal{E}}{n S_{\text{coil}} \pi f}$, where n and S_{coil} are the number of turns and surface of the pick-up coil and f the magnetic field frequency. The value of the product $n S_{\text{coil}}$ was deduced from a calibration experiment, during which the pick-up coil was used to measure a high-frequency AMF of known value, measured using a gaussmeter (GM08, Hirst Magnetics). Magnetic simulations were performed using FEMM software. The magnetization curve of the ferrite core was introduced into the software using the constructor datasheet. It has been checked that simulation results weakly depend on the exact geometry and position of the coil and on the angle of the V-shape enlargement.

Electromagnet heating. In preliminary experiments performed in ambient air, temperature of medium and electromagnet during magnetic field operation were measured using an infrared camera (Thermal imager 885, Testo). A current $I = 1.5$ A was sent through the coil, similarly to experiments under microscope. Thermal images as a function of time in these conditions are shown in Figure S3(a). The thermal image after one hour of magnetic

field application is shown in Figure 1(d). Thermal image shows that electromagnet heating is mainly localized to the wires. The evolution of temperature with time is displayed in Figure S3(b) for three points : i) medium, ii) wires, and iii) ferrite close to the gap. The temperature difference between the ferrite near the gap and the medium does not exceed 1°C.

Nanoparticles synthesis and cell culture. The synthesis method and characterization of the magnetic nanopatform used in the present article have been described in details in Ref. [8]. The nanopatform (DY647-MNP-gastrin) is composed of commercial iron oxide nanoparticles coated with PEG-Amine (Gecco Dots, Sweden) and decorated with 100 molecules of a synthetic replicate of gastrin (Covalab) and 20 molecules of the fluorescent label NHS-DY647-PEG1 (Dyomics GmbH, Jena, Germany). The size of the magnetic core determined by transmission electron microscopy was 8.7 ± 1.6 nm. The specific absorption rate of these MNPs is 13 W/g at 275 kHz and 40 mT. The glucagon-producing hamster tumoral cell line INR1G9 stably expressing CCK2R (INR1G9-RCCK2) obtained as previously described [35] was cultured in RPMI 1640 medium containing 10% fetal bovine serum (FBS) and 100 units ml⁻¹ penicillin/streptomycin (Life technologies). Cells were grown in a humidified atmosphere at 95% air and 5% CO₂ at 37°C. 0.5×10^6 INR1G9-RCCK2 cells were seeded in 6-wells plates or in 35 mm diameter CELLview dishes (Greiner Bio-One) and grown overnight, incubated with DY647-MNP-gastrin (16 µg Fe ml⁻¹) for 24 hours at 37°C in RPMI 1640 buffered with 10 mM HEPES buffer pH 7.4 containing 0.5% FBS and 100 units/ml penicillin/streptomycin (incubation medium) to allow MNPs internalization and accumulation in lysosomes. Incubation medium was withdrawn and cells were rinsed twice with incubation medium. At this stage, magnetic measurements have shown that cells contain in average 2.2 pg of iron per cell which is actively targeted and accumulated into lysosomes [8].

Protocol for electromagnet operation under microscope. When performing experiments on adherent cells, the planarity of the gap is a crucial parameter and was adjusted by putting the electromagnet on an inverted reflected light microscope and by focusing on the gap bottom. Screws were then adjusted so the gap image is clearly defined on a width as large as possible, which is a sign of its planarity. The electromagnet was then put inside a CELLview dish (Greiner Bio-One) containing attached cells having incorporated MNPs. To perform experiments on cells included in soft agarose gel, cells having or not internalized MNPs during 24 hours were scrapped, rinsed with incubation medium and mixed with agarose at a final concentration of 0.5%, then poured into the gap of electromagnet in a 35 mm diameter CELLview dish. After gel solidification, the CELLview dish was completed with incubation medium. For all types of experiments, CELLview dish was then placed above the heating plate of the confocal microscope and a home-made environmental chamber was built using a thin glass plate for the top cover and play-dough for the walls. Small diameter glass tubes were used as go throughs for the Litz wires inside play-dough. A thermal probe (Reflex, Neoptix) was put inside the medium, as close as possible from the gap. In this configuration, applying a current of 1.5 A inside the driving coil brought the temperature of the medium to 34 °C. The temperature was rose to 37°C and maintained at this temperature by adjusting the heating power of the hot plate. AMF of amplitude 53 mT and frequency 300 kHz was applied for 90 to 120 minutes.

Determination of cell damage. INR1G9-RCCK2 cells having or not internalized DY647-MNP-gastrin were included in agarose gel containing $3 \mu\text{g ml}^{-1}$ propidium iodide, and poured into the electromagnet placed in a CELLView dish, as previously described. Cells were exposed to the AMF (53 mT, 300 kHz) for 120 minutes. After magnetic field application, CELLview was maintained in an incubator with humidified atmosphere at 95% air and 5% CO₂ at 37°C for 4 hours. Counting of propidium iodide-labeled cells (excitation wavelength:

543 nm) was carried out by analyzing confocal microscopy images of 200-400 cells/experiments using ImageJ software.

Lysosomal membrane permeabilization. INR1G9-RCCK2 cells having internalized DY647-MNP-gastrin were incubated with RPMI 1640 0.5% FBS containing 75 nM LysoTracker Red (Molecular probes, excitation wavelength: 543 nm) for 15 minutes, rinsed with incubation medium, included in agarose gel and poured into the gap of electromagnet, as previously described. Different positions presenting cells having incorporated MNPs were marked inside and outside the gap. Before and during application of AMF (53 mT, 300 kHz) for 90 minutes, lysosome integrity was monitored by analyzing the colocalization between DY647-MNP-gastrin and LysoTracker Red labeling of confocal microscopy images of the marked positions using Pearson's coefficient (ImageJ software). 20-30 cells/experiments were analyzed of four independent experiments.

Dynamic of ROS production. 0.5×10^6 INR1G9-RCCK2 cells were seeded in 35 mm diameter CELLview dishes (Greiner), grown overnight and incubated with DY647-MNP-gastrin ($16 \mu\text{g Fe ml}^{-1}$) for 24 hours at 37°C in incubation medium. Cells were rinsed with incubation medium, incubated with CellROX Green reagent (Molecular probes, Excitation wavelegnth: 488 nm) in incubation medium according to manufacturer's instructions. Different positions presenting cells having incorporated MNPs were marked inside and outside the gap. Before and during application of AMF (53 mT, 300 kHz) for 120 minutes, ROS production was monitored by analyzing the intensity of CellROX Green reagent labeling of confocal microscopy images of the marked positions using Morpho expert software (Explora Nova, la Rochelle, France). 2000-3000 cells/experiments were analyzed of four independent experiments.

Statistical analysis. Results are expressed as the mean \pm SEM. Statistical analysis was performed using Student's *t*-test or ANOVA. Differences were considered significant when $p < 0.05$.

Supporting Information

Supporting Information is available from the Wiley Online Library or from the author.

Acknowledgments.

This work was partly supported by the ITMO Cancer during the “Plan cancer 2009-2013”, by Ligue Nationale Contre le Cancer and by the European Community's Seventh Framework Program under grant agreement no. 262943 “MULTIFUN”. D. EHD. is supported by grants from Association pour la Recherche contre le Cancer and Club Français du Pancréas. We thank Renaud Mathevet for his help in building and calibrating the pick-up coil. V.C and P.C. contributed equally to this work. J.C. and V.G. contributed equally to this work.

Received: ((will be filled in by the editorial staff))

Revised: ((will be filled in by the editorial staff))

Published online: ((will be filled in by the editorial staff))

[1] I. Hilger, *Int. J. Hyp.* **2014**, *29*, 828.

[2] A. Meffre, B. Mehdaoui,, V. Kelsen, P. F. Fazzini, J. Carrey, S. Lachaize, M. Respaud, B. Chaudret, *Nanoletters* **2012**, *12*, 4722.

[3] P. Guardia, R. Di Corato, L. Lartigue, C. Wilhelm, A. Espinosa, M. Garcia-Hernandez, F. Gazeau, L. Manna, T. Pellegrino, *ACS Nano* **2012**, *6*, 3080.

[4] E. Alphantéry, S. Faure, O. Seksek, F. Guyot, I. Chebbi, *ACS Nano* **2011**, *5*, 6279.

-
- [5] J. Carrey, B. Mehdaoui, M. Respaud, *Journal of Applied Physics* **2011**, *109*, 083921.
- [6] M. Creixell, A. C. Bohorquez, M. Torres-Lugo, C. Rinaldi, *ACS Nano* **2011**, *5*, 7124.
- [7] M. Domenech, I. Marrero-Berrios, M. Torres-Lugo, C. Rinaldi, *ACS Nano* **2013**, *7*, 5091.
- [8] C. Sanchez, D. El Hajj Diab, V. Connord, P. Clerc, E. Meunier, B. Pipy, B. Payré, J. Carrey, V. Gigoux, D. Fourmy, *ACS Nano* **2014**, *8*, 1350
- [9] A. Villanueva, P. de la Presa, J. M. Alonso, T. Rueda, A. Martinez, P. Crespo, M. P. Morales, M. A. Gonzalez-Fernandez, J. Valdes, G. Rivero, *J. Phys. Chem. C* **2010**, *114*, 1976.
- [10] G. F. Goya, L. Asín, M. R. Ibarra, *International Journal of Hyperthermia* **2013**, *29*, 810.
- [11] C. L. Dennis, A. J. Jackson, J. A. Borchers, P. J. Hoopes, R. Strawbridge, A. R. Foreman, J. van Lierop, C. Grüttner, R. Ivkov, *Nanotechnology* **2009**, *20*, 395103.
- [12] T.-J. Li, C.-C. Huang, P.-W. Ruan, K.-Y. Chuang, K.-J. Huang, D.-B Shieh, C.-S. Yeh, *Biomaterials* **2013**, *34*, 7873.
- [13] H.-Y. Tseng, G.-B. Lee, C.-Y. Lee, Y.-H. Shih, X.-Z. Lin, *IET Nanobiotechnology* **2009**, *3*, 46.
- [14] M. Kettering, H. Richter, F. Wiekhorst, S. Bremer-Streck, L. Trahms, W. A. Kaiser, I. Hilger, *Nanotechnology* **2011**, *22*, 505102.

-
- [15] L. Lartigue, D. Alloyeau, J. Kolosnjaj-Tabi, Y. Javed, P. Guardia, A. Riedinger, C. P  choux, T. Pellegrino, C. Wilhelm, F. Gazeau, *ACS Nano* **2013**, 7, 3939.
- [16] G. Graz  , A. M. Silber, M. Moros, L. As  n, T. E. Torres, C. Marquina, M. R. Ibarra, G. F. Goya, *International Journal of Nanomedicine* **2012**, 5351.
- [17] B. Kozissnik, A. C. Bohorquez, J. Dobson, C. Rinaldi, *International Journal of Hyperthermia* **2013**, 29, 706.
- [18] F. Vetrone, R. Naccache, A. Zamarr  n, A. Juarranz de la Fuente, F. Sanz-Rodr  guez, L. Martinez Maestro, E. Mart  n Rodriguez, D. Jaque, J. Garc  a Sol  , J. A. Capobianco, *ACS Nano* **2010**, 4, 3254.
- [19] M. P. Alvarez-Berrios, A. Castillo, J. Mendez, O. Soto, C. Rinaldi, M. Torres-Lugo, *International Journal of Nanomedicine* **2013**, 8, 1003.
- [20] L.-M. Lacroix, J. Carrey, M. Respaud, *Review of Scientific Instruments* **2008**, 79, 093909.
- [21] T. Sadhukha, L. Niu, T. S. Wiedmann, J. Panyam, *Molecular Pharmaceutics* **2013**, 10, 1432.
- [22] M. A. Voinov, J. O. Sosa Pag  n, E. Morrison, T. I. Smirnova, A. I. Smirnov, *J. Am. Chem. Soc.* **2011**, 133, 35–41
- [23] E. Zhang, M. F. Kircher, M. Koch, L. Eliasson, S. N. Goldberg, E. Renstr  m, *ACS Nano* **2014**, 8, 3192.

-
- [24] J. Carrey, V. Connord, M. Respaud, *Applied Physics Letters* **2013**, *102*, 232404.
- [25] H. Huang, S. Delikanli, H. Zeng, D. M. Ferkey, A. Pralle, *Nature Nanotechnology* **2010**, *5*, 602.
- [26] L. Polo-Corrales, C. Rinaldi, *Journal of Applied Physics* **2012**, *111*, 07B334.
- [27] A. Riedinger, P. Guardia, A. Curcio, M. A. Garcia, R. Cingolani, L. Manna, T. Pellegrino, *Nano Letters* **2013**, *13*, 2399.
- [28] J. Dong, J. I. Zink, *ACS Nano* **2014**, *8*, 5199.
- [29] Y. Chen, A. Bose, G. D. Bothun, *ACS Nano* **2010**, *4*, 3215.
- [30] M. Pernia Leal, A. Torti, A. Riedinger, R. La Fleur, D. Petti, R. Cingolani, R. Bertacco, T. Pellegrino, *ACS Nano* **2012**, *6*, 10535.
- [31] C. Sanson, O. Diou, J. Thévenot, E. Ibarboure, A. Soum, A. Brûlet, S. Miraux, E. Thiaudière, S. Tan, A. Brisson, V. Dupuis, O. Sandre, S. Lecommandoux, *ACS Nano* **2011**, *5*, 1122.
- [32] S. Brulé, M. Levy, C. Wilhelm, D. Letourneur, F. Gazeau, C. Ménager, C. Le Visage, *Advanced Materials* **2011**, *23*, 787.
- [33] M. Yamaguchi, A. Ito, A. Ono, Y. Kawabe, M. Kamihira, *ACS Synthetic Biology* **2014**, *3*, 273.

[34] N. L. Klyachko, M. Sokolsky-Papkov, N. Pothayee, M. V. Efremova, D. A. Gulin, N. Pothayee, A. A. Kuznetsov, A. G. Majouga, J. S. Riffle, Y. I. Golovin, A. V. Kabanov, *Angewandte Chemie International Edition* **2012**, *51*, 12016.

[35] S. Leung-Theung-Long, E. Roulet, P. Clerc, C. Escrieut, S. Marchal-Victorion, B. Ritz-Laser, J. Philippe, L. Pradayrol, C. Seva, D. Fourmy, M. Dufresne, *Journal of Biological Chemistry* **2005**, *280*, 7976.

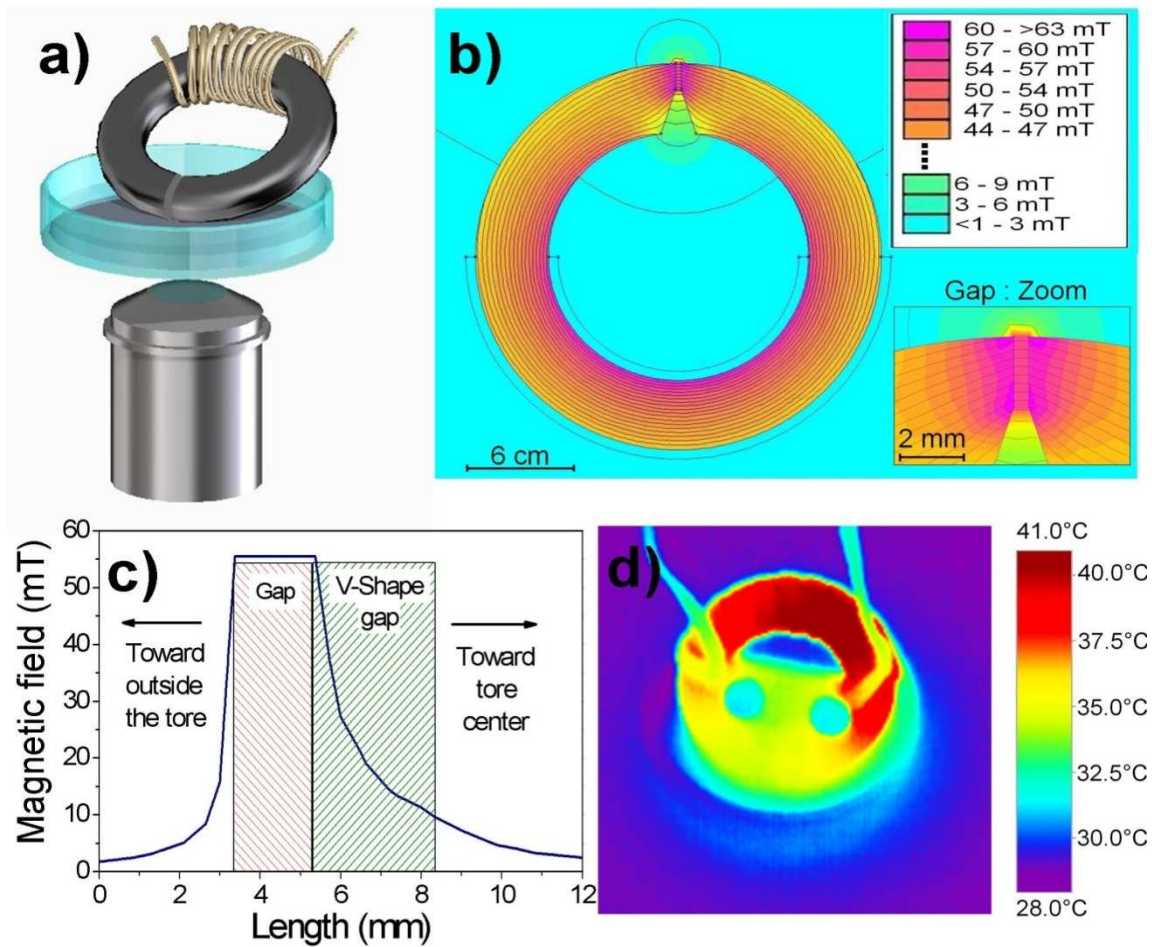


Figure 1: Description of the miniaturized electromagnet. (a) Schematic of the setup. (b) Magnetic field intensity map calculated using FEMM software. Inset shows an enlargement of the gap. (c) Magnetic field intensity as a function of the position inside the gap deduced from FEMM software. The $400\ \mu\text{m}$ width gap zone where the cells are located is labeled as “gap”. The V-shape zone enlarged to avoid shadowing of the gap is labeled as “V-shape gap”. (d) Infrared camera picture of the electromagnet and of a CELLview containing some medium taken after one hour of AMF application.

DY647-MNP-gastrin / Propidium iodide

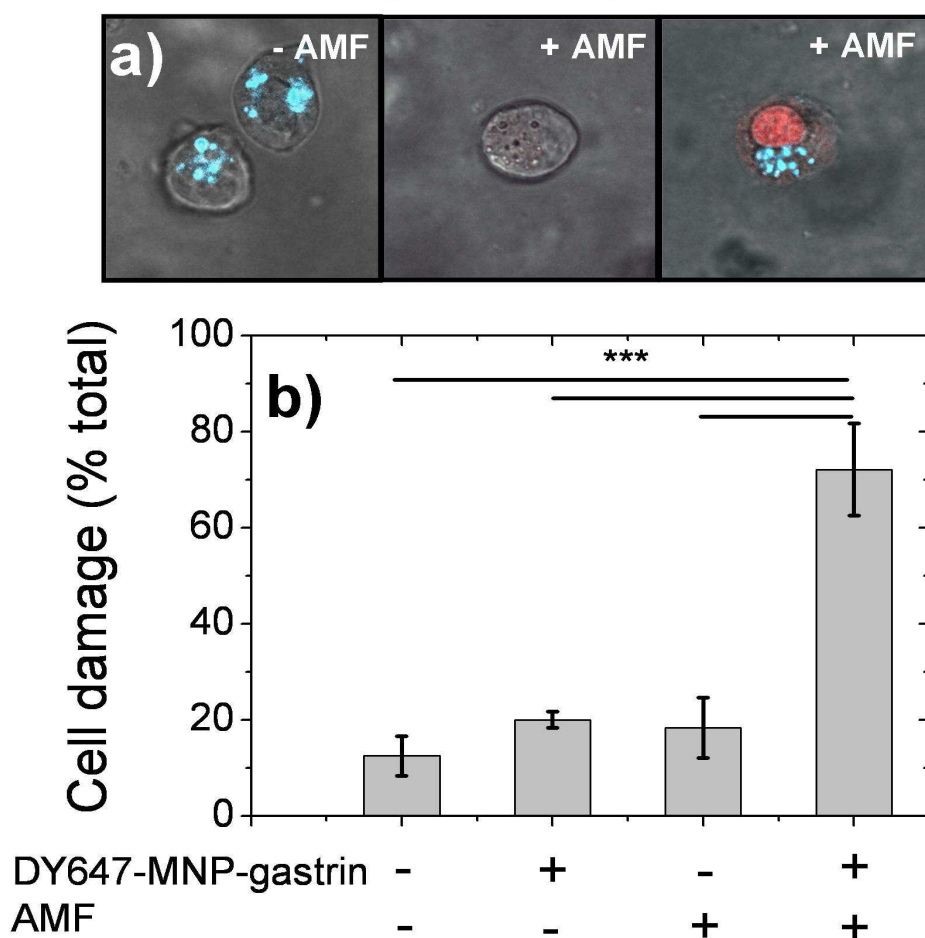


Figure 2: Alternating magnetic field induces specifically damage to cells having internalized MNPs. INR1G9-RCCK2 cells having or not internalized DY647-MNP-gastrin were included in agarose gel containing $3 \mu\text{g ml}^{-1}$ propidium iodide and poured in the gap of the electromagnet. Cells were exposed to the AMF (53 mT, 300 kHz) for 120 mn. After AMF application, CELLview was maintained in an incubator with humidified atmosphere at 37°C for 4 hours. (a) Confocal microscopy images illustrate the propidium iodide labeling of cells submitted (+AMF) or not (-AMF) to the magnetic field: cells with a damaged membrane were labeled by propidium iodide. (b) Cells having a damaged membrane were counted 4 hours after the end of AMF exposure by confocal microscopy analysis of cells labeled with propidium iodide. The distinction is made between cells inside and outside the gap as well as cells having or not internalized DY647-MNP-gastrin. Results are mean \pm SEM of four separate experiments. Statistical analysis performed using ANOVA; *** $p < 0.001$.

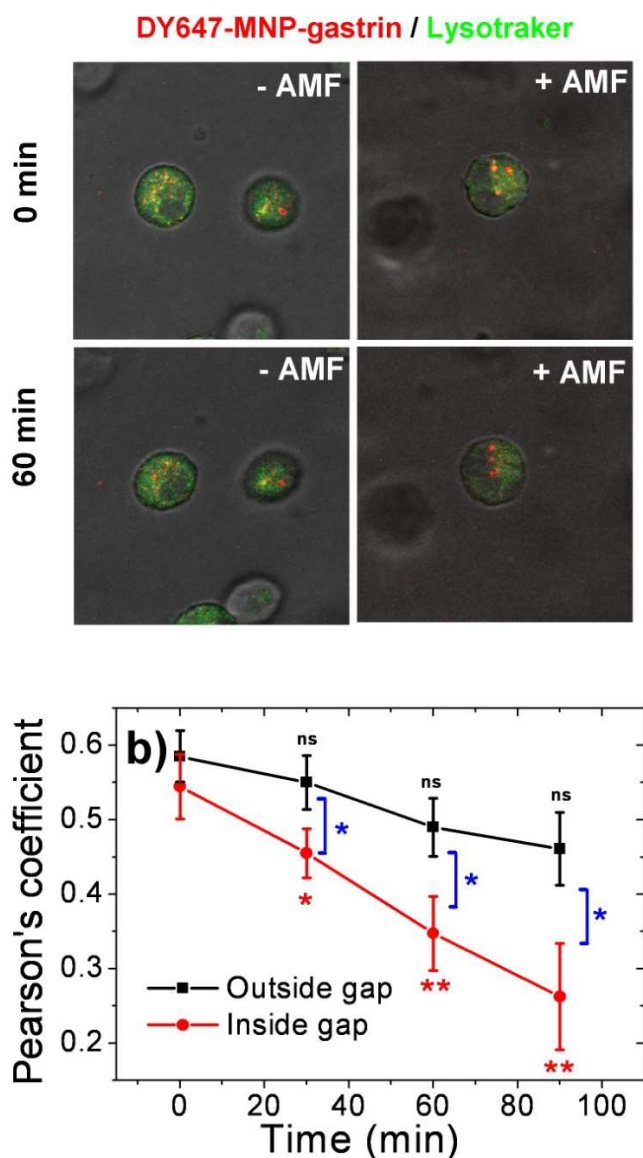


Figure 3: Application of alternating magnetic field affected lysosome integrity of cells having internalized DY647-MNP-gastrin. INR1G9-RCCK2 cells having internalized DY647-MNP-gastrin and accumulated LysoTracker Red were rinsed, included in agarose gel and poured in the gap of the electromagnet. Different positions presenting cells having incorporated MNPs were marked inside and outside the gap. (a) Confocal microscopy images illustrate the lysosome integrity of cells outside (-AMF) and inside (+AMF) the gap of electromagnet. (b) Before and during AMF application (53 mT, 300 kHz) for 90 min, lysosome integrity was monitored by analyzing the colocalization between DY647-MNP-gastrin and LysoTracker Red labeling of the confocal microscopy images of the marked positions using Pearson's coefficient (ImageJ software). 20-30 cells/experiments were analyzed of four independent experiments. Statistical analysis performed using ANOVA: in red and black, *versus* $t=0$; in blue, inside *versus* outside the gap; * $p < 0.05$, ** $0.01 < p < 0.05$.

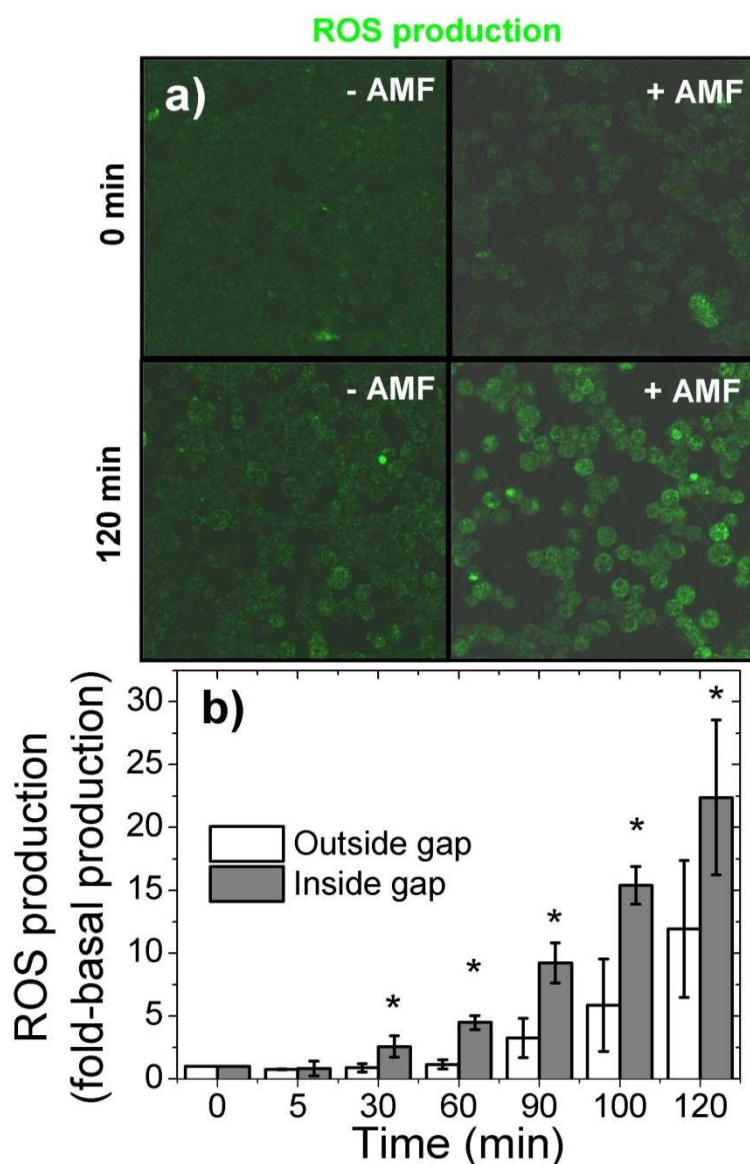


Figure 4: Applying a magnetic field on adherent cells containing DY647-MNP-gastrin increases ROS production. INR1G9-RCCCK2 cells having internalized DY647-MNP-gastrin were rinsed and incubated with CellROX Green reagent. Different positions presenting cells having incorporated MNPs were marked inside (+AMF) and outside (-AMF) the gap. (a) Confocal microscopy images illustrate the ROS production before and at the end of AMF treatment. (b) Before and during application of AMF, ROS production was measured by analyzing the intensity of CellROX Green reagent labeling of confocal microscopy images of the marked positions. Statistical analysis performed using Student's *t*-test; $p < 0.05$, ** $0.01 < p < 0.05$.

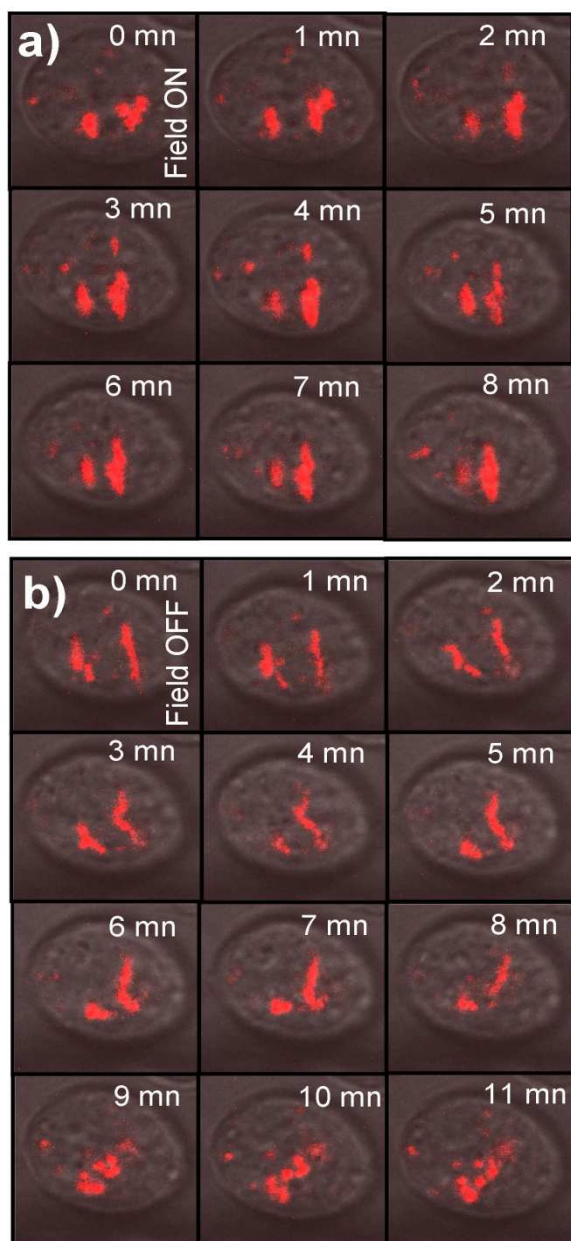


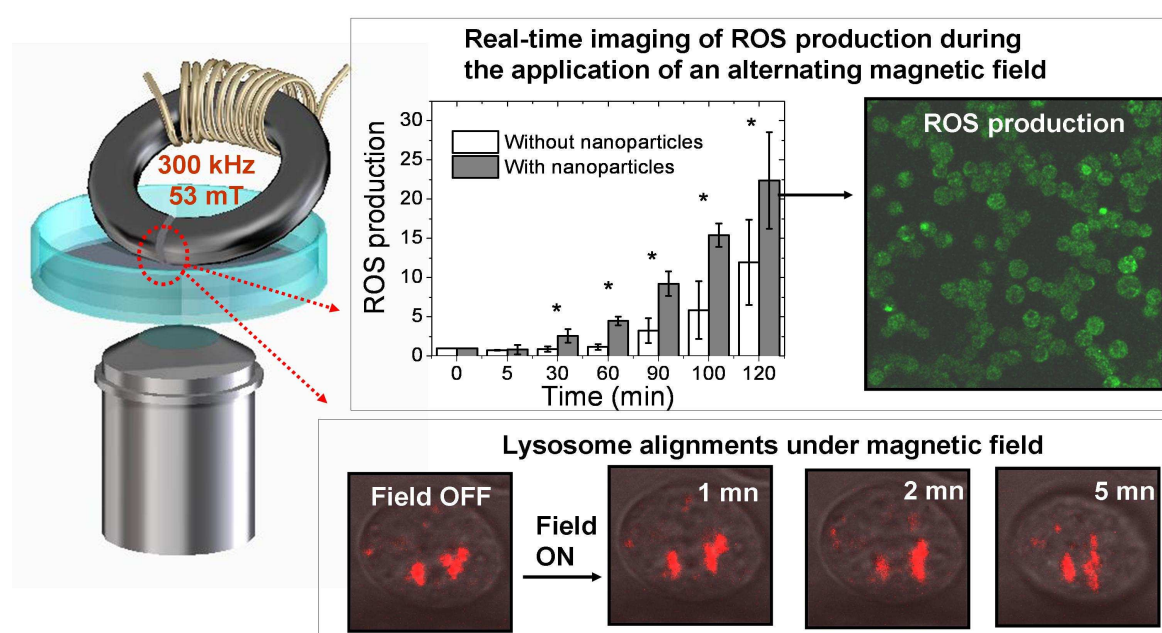
Figure 5 : Applying a magnetic field to some cells containing DY647-MNP-gastrin induces alignment of the lysosomes. Evolution of the spatial repartition of DY647-MNP-gastrin inside a single cell when AMF is switched on and off. A z-stack acquisition containing 7 or 8 pictures was taken every minute on the cell, with a total acquisition time of 34 s. To draw this figure, a single picture was chosen from the z-stack to ensure a good visualization of DY647-MNP-gastrin. The field is switched (a) ON (b) OFF between the first and the second picture.

A miniaturized electromagnet makes possible the generation of a high-frequency magnetic field under a confocal microscope. Several physical and biological events occurring in cells containing magnetic nanoparticles and submitted to such a field are observed and quantified in real-time : cell damages, reactive oxygen species production, lysosome permeabilization and nanoparticles self-assembling.

magnetic nanoparticles, magnetic hyperthermia, confocal microscope, cell death, reactive oxygen species

V. Connord[#], P. Clerc[#], N. Hallali, D. El Hajj Diab, D. Fourmy, V. Gigoux* and J. Carrey*

Real-time Analysis of Magnetic Hyperthermia Experiments on Living Cells under Confocal Microscope



Copyright WILEY-VCH Verlag GmbH & Co. KGaA, 69469 Weinheim, Germany, 2013.

Supporting Information

Real-time Analysis of Magnetic Hyperthermia Experiments on Living Cells under Confocal Microscope

Vincent Connord[#], Pascal Clerc[#], Nicolas Hallali, Darine El Hajj Diab, Daniel Fourmy, Véronique Gigoux, and Julian Carrey**

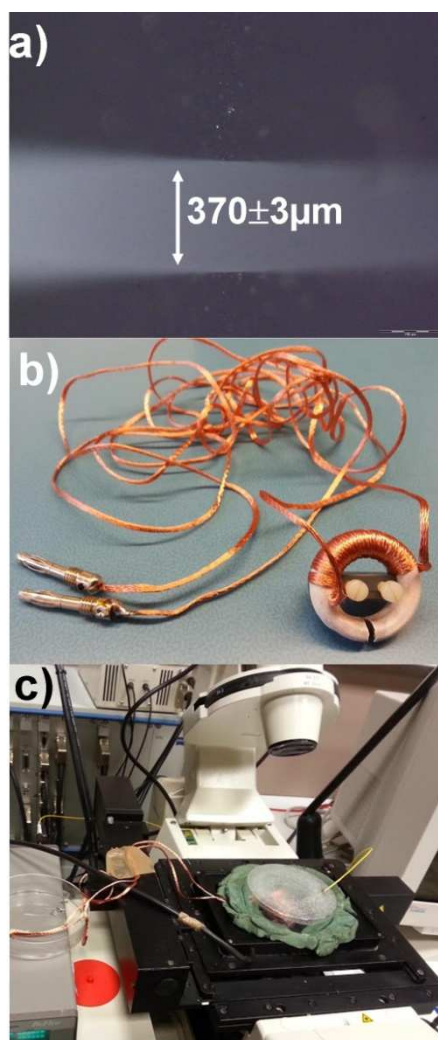


Figure S1 : Pictures of the miniaturized electromagnet.

(a) Picture at the edge of the gap taken using an inverted microscope. (b) Picture of the whole electromagnet. (c) Picture of the setup under confocal microscope

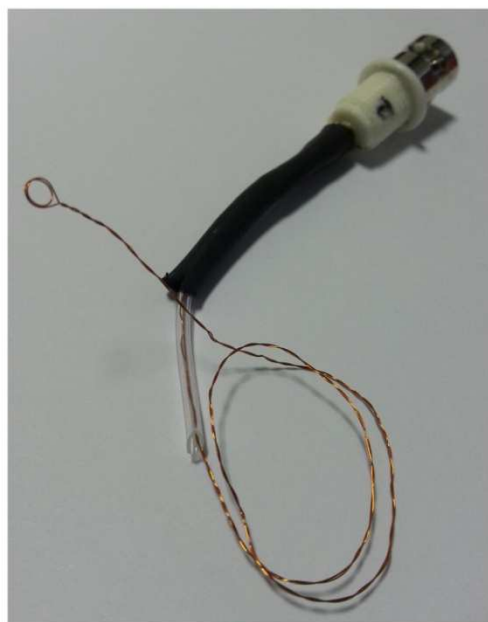


Figure S2 : Picture of the pick-up coil used to measure the AMF amplitude inside the gap of the electromagnet.

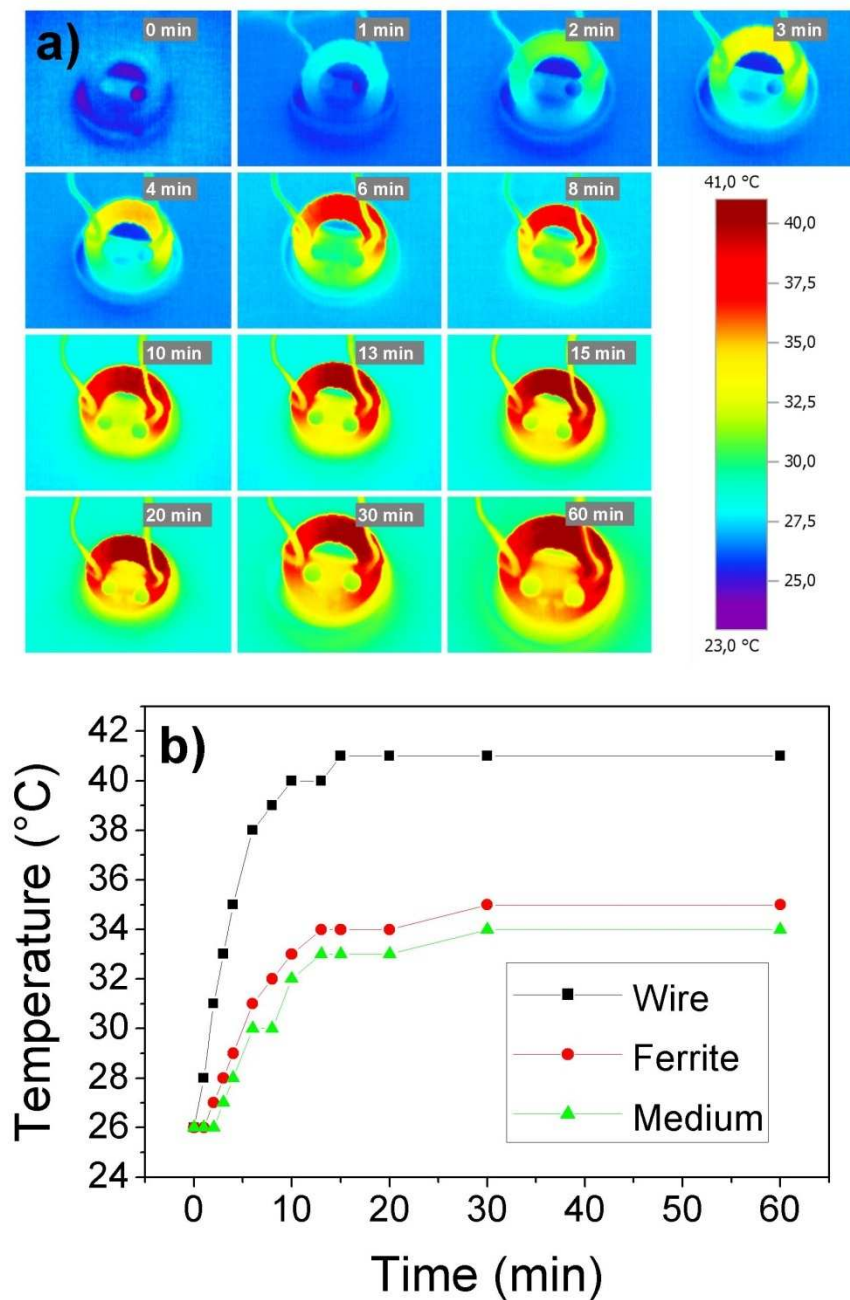


Figure S3 : (a) Evolution with time of the electromagnet and medium temperature when applying the magnetic field, followed by infrared camera. These experiments were performed in ambient air. (b) Evolution of the temperature in three points of the previous pictures: (■) the wire; (●) the ferrite near the medium; (▲) the medium.